Reactions of Laser-Ablated Iron Atoms with Halomethanes: Infrared Spectra, Density Functional Calculations, and Structures of Simple Iron Insertion and Methylidene Complexes

Han-Gook Cho,[†] Jonathan T. Lyon,[‡] and Lester Andrews*[,‡]

Departments of Chemistry, University of Incheon, 177 Dohwa-dong, Nam-ku, Incheon 402-749, South Korea, and University of Virginia, P.O. Box 400319, Charlottesville, Virginia 22904−4319

Received June 5, 2008

Reactions of laser-ablated Fe atoms with halomethanes and ethane have been investigated through matrix infrared spectra and density functional calculations. Only insertion complexes are identified from reactions of Fe with methyl fluoride and ethane, parallel to the previously observed insertion complex CH_3-FeH from the photochemical reaction with methane. However, Fe also forms methylidene complexes through α-X migration in the insertion products from Fe reactions with di-, tri-, and tetrahalomethanes. Calculated structures show no agostic distortion in these methylidene complexes. However, an interesting distortion and elongation of the C−Cl bond is observed in the Fe insertion products, such as $H_2ClC-FeCl$, while no such distortion of the C−H or C−F bond is found in analogous calculated structures for $H_2FC-FeCl$. This distortion is likely due to a Cl lone pair to Fe bonding interaction that ultimately leads to formation of the lower energy $CH_2{=}FeCl_2$ methylidene complex. This Cl atom transfer is reversible on visible−ultraviolet irradiation. There is no evidence for methylidyne complexes of the type recently observed for Ru, as such higher oxidation state structures become more stable on going down the family group.

Introduction

The discovery of high-oxidation-state transition-metal complexes in the 1970s[1,2] greatly expanded the horizon of coordination chemistry and the understanding of carbon−metal multiple bonds. Their rich chemistry includes distinctive structures as well as growing applications in various syntheses, particularly C−H insertion and catalytic metathesis reactions.[3] Among the numerous high-oxidation-state complexes provided through a variety of synthetic routes, relatively small numbers of Fe and Ru derivatives have been produced,[1,4−7] and therefore, their structural and photochemical properties remain largely unknown. Cyclopentadienyldicarbonyliron carbene complexes are used to provide highly stereoselective synthetic routes and reactions with olefins to form asymmetric cyclopropanes through backside ring closure.[4a,b]

Oxidative C−H insertion of CH_4 by Fe occurs during photolysis after codeposition of the reactants, forming the insertion complex (CH_3-FeH), but further rearrangement to higher oxidation state complexes is not observed.[8] In addition, both $FeCH_2$ and HFeCH have been identified from reactions of Fe with CH_2N_2 and subsequent photolysis.[9] In addition, Ru insertion or methylidene complexes are also produced in reactions of Ru with halomethanes along with the methylidyne complex, while only the insertion complex is identified from reactions with methane.[10] All three types of complexes were observed in group 6 metal atom reactions, with the established

* To whom correspondence should be addressed. E-mail: lsa@virginia.edu.

[†] University of Incheon.

[‡] University of Virginia.

(1) (a) Herndon, J. W. *Coord. Chem. Rev.* **2007**, *251*, 1158. (b) Herndon, J. W. *Coord. Chem. Rev.* **2006**, *250*, 1889. (c) Herndon, J. W. *Coord. Chem. Rev.* **2005**, *249*, 999. (d) Herndon, J. W. *Coord. Chem. Rev.* **2004**, *248*, 3. (e) Schrock, R. R. *Chem. Rev.* **2002**, *102*, 145.

(2) (a) Fischer, E. O.; Kreis, G.; Kreiter, C. G.; Müller, J.; Huttner, G.; Lorenz, H. *Angew. Chem., Int. Ed. Engl.* **1973**, *12*, 564. (b) McLain, S. J.; Wood, C. D.; Messerle, L. W.; Schrock, R. R.; Hollander, F. J.; Youngs, W. J.; Churchill, M. R. *J. Am. Chem. Soc.* **1978**, *100*, 5962.

(3) (a) Grubbs, R. H., Ed. *Handbook of Metathesis*; Wiley-VCH: Weinheim, Germany, 2003; Vols. *1 and 3*. (b) Bunz, U. H. F. *Chem. Rev.* **2000**, *100*, 1605. (c) Nugent, W. A.; Mayer, J. M. *Metal-Ligand Multiple Bonds*; Wiley: New York, 1988. (d) See article on iron as a catalyst in: *Chem. Eng. News* **2008**, July 28, 53.

(4) (a) Ishii, S.; Zhao, S.; Helquist, P. *J. Am. Chem. Soc.* **2000**, *122*, 5897, and references therein. (b) Wang, Q.; Försterling, F. H.; Hossain, M. M. *J. Organomet. Chem.* **2005**, *690*, 6238. (c) Zhang, S.; Xu, Q.; Sun, J.; Chen, J. *Chem. Eur. J.* **2003**, *9*, 5111. (d) Brookhart, M.; Studabaker, W. B. *Chem. Rev.* **1987**, *87*, 411. (e) Kremer, K. A. M.; Kuo, G.-H.; O′Conner, E. J.; Helquist, P.; Kerber, R. C. *J. Am. Chem. Soc.* **1982**, *104*, 6119(Fe carbenes).

(5) (a) Fischer, E. O.; Schneider, J.; Neugebauer, D. *Angew. Chem.* **1984**, *96*, 814. (b) Grady, W. L.; Bursey, M. M. *Int. J. Mass Spectrom. Ion Processes* **1984**, *56*, 161 (Fe^+ carbyne intermediates).

(6) (a) Gallop, M. A.; Roper, W. R. *Adv. Organomet. Chem.* **1986**, *25*, 121. (b) Coalter, J. N.; Bollinger, J. C.; Eisenstein, O.; Caulton, K. G. *New J. Chem.* **2000**, *24*, 925. (c) Sanford, M. S.; Henling, L. M.; Day, M. W.; Grubbs, R. H. *Angew. Chem., Int. Ed.* **2000**, *39*, 3451. (d) Gonzales-Herrero, P.; Weberndorfer, B.; Ilg, K.; Wolf, J.; Werner, H. *Angew. Chem., Int. Ed.* **2000**, *39*, 3266. (e) Gonzales-Herrero, P.; Weberndorfer, B.; Ilg, K.; Wolf, J.; Werner, H. *Organometallics* **2001**, *20*, 3672. (f) Amoroso, D.; Snelgrove, J. L.; Conrad, J. C.; Droulin, S. D.; Yap, G. P. A.; Fogg, D. E. *Adv. Synth. Catal.* **2002**, *344*, 757 (Ru carbyne synthesis).

(7) (a) Fischer, H.; Hofmann, P.; Kreissl, F. R.; Schrock, R. R.; Schubert, U.; Weiss, K. *Carbyne Complexes*; VCH: New York, 1988. (b) Gallop, M. A.; Roper, W. R. *Adv. Organomet. Chem.* **1986**, *25*, 121. (c) Engel, P. F.; Pfeffer, M. *Chem. Rev.* **1995**, *95*, 2281.

(8) (a) Billups, W. E.; Konarski, M. M.; Hauge, R. H.; Margrave, J. L. *J. Am. Chem. Soc.* **1980**, *102*, 7393. (b) Ozin, G. A.; McCaffrey, J. G. *Inorg. Chem.* **1983**, *22*, 1397. (c) Kafafi, Z. H.; Hauge, R. H.; Margrave, J. L. *J. Am. Chem. Soc.* **1985**, *107*, 6134. (d) Yamada, Y.; Katsumata, K.; Shimasaki, H.; Ono, Y.; Yamaguchi, K *Bull. Chem. Soc. Jpn.* **2002**, *75*, 277 (Fe + CH_4).

(9) (a) Chang, S.-C.; Hauge, R. H.; Kafafi, Z. H.; Margrave, J. L. *J. Am. Chem. Soc.* **1988**, *110*, 7975. (b) Chang, S.-C.; Kafafi, Z. H.; Hauge, R. H.; Billups, W. E.; Margrave, J. L. *J. Am. Chem. Soc.* **1985**, *107*, 1447 (Fe + CH_2N_2).

(10) Cho, H.-G.; Andrews, L. *Eur. J. Inorg. Chem.* **2008**, 2537 (Ru + $CH(X)_4$).

10.1021/om8005189 CCC: $40.75
Publication on Web 09/26/2008

trend of increased stability for higher oxidation states going down the family group.[11] Osmium fits this premise, as the exclusive formation of Os methylidynes is found in reactions of Os with CH_4, C_2H_6, and CH_3X, showing high preference for the carbon−osmium triple bond.[12]

The importance of C−H activation continues to increase in synthetic and industrial chemistry.[4,13,14] Recently a new breed of simple high-oxidation-state complexes has been introduced by activation of small alkanes and halomethanes with laser-ablated transition-metal atoms, many of which show unique structures and reversible photochemistry.[15] Here, we report the IR spectra of isotopic products from reactions of laser-ablated Fe atoms with halomethanes and ethane. The insertion and carbene products are identified depending on the system. DFT computations reveal unique structures for the products, and the structural effects of the chlorine lone electron pair on the metal center are examined for these simple complexes.

Experimental and Computational Methods

Laser-ablated Fe (Johnson-Matthey) atoms were reacted with CH_3F (Matheson), CD_3F (synthesized from CD_3Br and HgF_2), $^{13}CH_3F$ (Cambridge Isotopic Laboratories, 99%), C_2H_6 (Matheson), C_2D_6 (MSD Isotopes), CH_2F_2, CD_2F_2,[16] CH_2FCl, CD_2FCl,[16] CH_2Cl_2, CD_2Cl_2, $^{13}CH_2Cl_2$, CHF_3, CDF_3,[16] $CHCl_3$, $CDCl_3$,[16] $^{13}CHCl_3$, CF_3Cl, $^{13}CF_3Cl$, CF_2Cl_2, CCl_4 (Dupont), and $^{13}CCl_4$ in excess argon during condensation at 10 K using a closed-cycle refrigerator (Air Products HC-2). These methods have been described in detail elsewhere.[17] Reagent gas mixtures ranged 0.5−1.0% in argon. After reaction, infrared spectra were recorded at a resolution of 0.5 cm^{-1} using a Nicolet 550 spectrometer with an MCT-B detector. Samples were later irradiated for 20 min periods by a mercury arc street lamp (175 W) with the globe removed and a combination of optical filters and subsequently annealed to allow further reagent diffusion.[17]

In order to support the assignment of new experimental frequencies, density functional theory (DFT) calculations were carried out using the Gaussian 03 package,[10−12,18] B3LYP density functional,[19] and 6-311++G(3df,3pd) basis sets for C, H, F, Cl, and Fe[20] to provide a consistent set of vibrational frequencies for the reaction products. Geometries were fully relaxed during optimization, and the optimized geometry was confirmed by vibrational analysis. BPW91[21] calculations were also done to complement the B3LYP results. The vibrational frequencies were calculated analytically, and the zero-point energy is included in the calculation of binding energies. The computed $\langle S(S+1)\rangle$ expectation values show that the triplet and quintet state reaction products are mixed spin states; thus, our DFT calculations are approximate and useful only as a general guide to facilitate identification of product spectra. Previous investigations have shown the DFT calculated harmonic frequencies are usually slightly higher than observed frequencies, depending on the mode anharmonicity,[10−12,15,22,23] but this is not always the case. The reader must appreciate that the calculation of vibrational frequencies is not an exact science, and these calculations provide useful predictions of infrared spectra of new molecules.

Results and Discussion

Reactions of iron atoms with halomethane and ethane isotopomers were carried out, and the matrix infrared spectra of new products will be compared with frequencies for low-energy product structures calculated by density functional theory. Spectra from similar experiments with other laser-ablated metals and these same precursors were examined to make sure that the new absorptions considered here are unique to the iron and precursor molecule reaction.[10,11]

Fe + CH_3F. Shown in Figure 1 are the CH_3F spectra in the Fe−F stretching and CH_3 rocking regions. The observed frequencies of the product absorptions are given in Table 1 and compared with the predicted values in Table S1 (Supporting Information). Previous studies show that reactions of metal atoms with small alkanes and halomethanes generate small metal complexes (insertion, carbene, and carbyne products).[15] The product absorptions marked **i** (for insertion product) are increased from their original intensities about 5 and 30% and slightly more on visible ($\lambda > 420$ nm), UV ($240 < \lambda < 380$ nm), and full arc ($\lambda > 220$ nm) irradiations, respectively. The sharp strong absorption at 662.3 cm^{-1}, showing small D and ^{13}C shifts of −7.2 and −1.2 cm^{-1}, is attributed to the Fe−F stretching mode of CH_3−FeF. The group of absorptions at 581.0, 578.6, 577.1, and 574.5 cm^{-1} along with similarly split D and ^{13}C counterparts (D and ^{13}C shifts of −135.3 and −3.6 cm^{-1}) are assigned to the degenerate CH_3 rocking modes of CH_3−FeF with C_{3v} symmetry. The good agreement with the DFT values in Table S1, as marked by the strong Fe−F stretching mode falling between the B3LYP and BPW91 values, while the predicted CH_3 rocking frequencies are slightly lower, substantiates formation of the insertion product. No other product absorptions are observed, and formation of the insertion complex is consistent with the previously reported observation of CH_3−FeH in photochemical reactions of Fe atoms and methane.[8] DFT calculations also show that the insertion complex is most stable among the plausible products: CH_3−FeF (Q), CH_2═FeHF (T), and HC≡FeH_2F (S) are 50 and 20 kcal/mol lower and 5 kcal/mol higher in energy than the reactants, respectively. (Here, Q, T, and S denote quintet, triplet, and

(11) Lyon, J. T.; Cho, H.-G.; Andrews, L. *Organometallics* **2007**, *26*, 6373 (Cr, Mo, W + CH_2X_2, CHX_3, CX_4).

(12) (a) Cho, H.-G.; Andrews, L. *Organometallics* **2008**, *27*, 1786 (Os + CH_4, C_2H_6, CH_3X). (b) Cho, H.-G.; Andrews, L. *Organometallics* **2007**, *26*, 4098. (c) Cho, H.-G.; Andrews, L. *Inorg. Chem.* **2008**, *47*, 1653 (Re + alkanes). (d) Lyon, J. T.; Cho, H.-G.; Andrews, L.; Hu, H.-S.; Li, J. *Inorg. Chem.* **2007**, *46*, 8728 (Re + CHX_3, CX_4).

(13) Díaz-Requejo, M. M.; Belderrain, T. R.; Nicasio, M. C.; Pérez, P. *Dalton Trans.* **2006**, *5559*.

(14) Campos, K. R. *Chem. Soc. Rev.* **2007**, *36*, 1069.

(15) Andrews, L.; Cho, H.-G. *Organometallics* **2006**, *25*, 4040, and references therein (review article).

(16) Isotopic modifications synthesized: Andrews, L.; Willner, H.; Prochaska, F. T. *J. Fluorine Chem.* **1979**, *13*, 273.

(17) (a) Andrews, L.; Citra, A. *Chem. Rev.* **2002**, *102*, 885, and references therein. (b) Andrews, L. *Chem. Soc. Rev.* **2004**, *33*, 123, and references therein.

(18) Kudin, K. N.; Burant, J. C.; Millam, J. M.; Iyengar, S. S.; Tomasi, J.; Barone, V.; Mennucci, B.; Cossi, M.; Scalmani, G.; Rega, N.; Petersson, G. A.; Nakatsuji, H.; Hada, M.; Ehara, M.; Toyota, K.; Fukuda, R.; Hasegawa, J.; Ishida, M.; Nakajima, T.; Honda, Y. ; Kitao, O.; Nakai, H.; Klene, M.; Li, X.; Knox, J. E.; Hratchian, H. P.; Cross, J. B.; Adamo, C.; Jaramillo, J.; Gomperts, R.; Stratmann, R. E.; Yazyev, O.; Austin, A. J.; Cammi, R.; Pomelli, C.; Ochterski, J. W.; Ayala, P. Y.; Morokuma, K.; Voth, G. A.; Salvador, P.; Dannenberg, J. J.; Zakrzewski, V. G.; Dapprich, S.; Daniels, A. D.; Strain, M. C.; Farkas, O.; Malick, D. K.; Rabuck, A. D.; Raghavachari, K.; Foresman, J. B.; Ortiz, J. V.; Cui, Q.; Baboul, A. G.; Clifford, S.; Cioslowski, J.; Stefanov, B. B.; Liu, G.; Liashenko, A.; Piskorz, P.; Komaromi, I.; Martin, R. L.; Fox, D. J.; Keith, T.; Al-Laham, M. A.; Peng, C. Y.; Nanayakkara, A.; Challacombe, M.; Gill, P. M. W.; Johnson, B.; Chen, W.; Wong, M. W.; Gonzalez, C.; Pople, J. A. Gaussian 03, Revision B.04; Gaussian, Inc., Pittsburgh, PA, 2003.

(19) (a) Becke, A. D. *J. Chem. Phys.* **1993**, *98*, 5648. (b) Lee, C.; Yang, Y.; Parr, R. G. *Phys. Rev. B* **1988**, *37*, 785.

(20) Raghavachari, K.; Trucks, G. W. *J. Chem. Phys.* **1989**, *91*, 1062.

(21) Burke, K.; Perdew, J. P.; Wang, Y. In *Electronic Density Functional Theory: Recent Progress and New Directions*; Dobson, J. F., Vignale, G., Das, M. P., Eds.; Plenum: New York, 1998.

(22) Cho, H.-G.; Andrews, L. *Organometallics* **2005**, *24*, 5678 (Cr, Mo, W + CH_3F).

(23) (a) Scott, A. P.; Radom, L. *J. Phys. Chem.* **1996**, *100*, 16502. (b) Andersson, M. P.; Uvdal, P. L. *J. Phys. Chem. A* **2005**, *109*, 3937.

Table 1. Frequencies of Product Absorptions (Group i) Observed from Reactions of Fe with Methyl Fluoride and Ethane Isotopomers in Excess Argon[a]

CH_3F	CD_3F	$^{13}CH_3F$	C_2H_6	C_2D_6	description
662.3	655.1	661.1			CH_3 rock
581.0, 578.6, 577.1, 574.5	445.7, 443.0, 441.3	577.4, 575.0, 573.5, 541.3	1662.8, 1660.5	1204.0, 1196.8	Fe−X(H) str
			482.9		C−Fe str

[a] All frequencies are in cm^{-1}. The description gives the major coordinate, and **i** stands for insertion products.

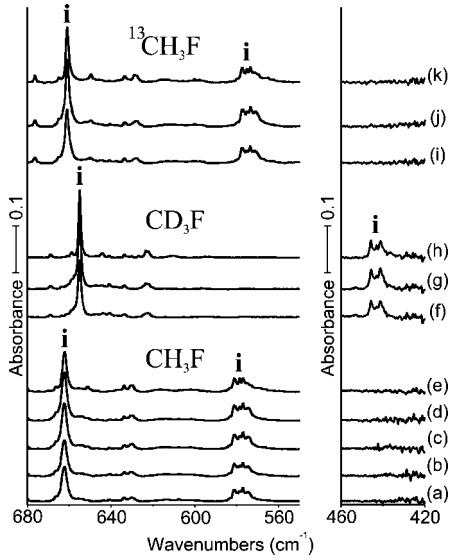

Figure 1. IR spectra in the regions of 680−550 and 460−420 cm^{-1} for laser-ablated Fe atoms codeposited with CH_3F isotopomers in excess argon at 10 K and their variation: (a) Fe + 0.5% CH_3F in Ar codeposited for 1 h; (b) as in (a) after photolysis ($\lambda > 420$ nm); (c) as in (b) after photolysis ($240 < \lambda > 380$ nm); (d) as in (c) after photolysis ($\lambda > 220$ nm); (e) as in (d) after annealing to 28 K; (f) Fe + 0.5% CD_3F in Ar codeposited for 1 h; (g) as in (f) after photolysis ($240 < \lambda < 380$ nm); (h) as in (g) after annealing to 28 K; (i) Fe + 0.5% $^{13}CH_3F$ in Ar codeposited for 1 h; (j) as in (i) after photolysis ($240 < \lambda < 380$ nm); (k) as in (j) after annealing to 28 K. **i** denotes the product absorption.

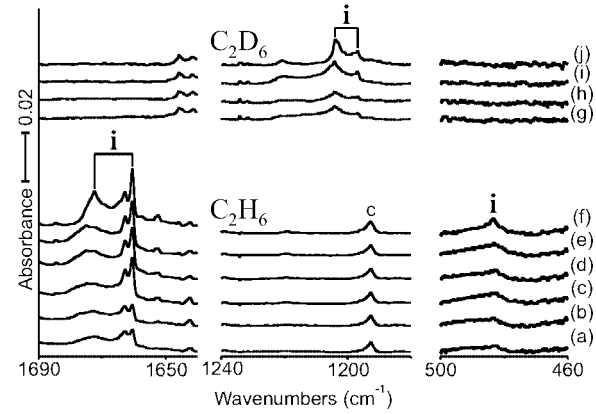

Figure 2. IR spectra in selected regions of 1690−1640, 1240−1180, and 500−460 cm^{-1} for laser-ablated Fe atoms codeposited with C_2H_6 and C_2D_6 in excess argon at 10 K and their variation: (a) Fe + 1.0% C_2H_6 in Ar codeposited for 1 h; (b) as in (a) after photolysis ($\lambda > 420$ nm); (c) as in (b) after photolysis ($240 < \lambda < 380$ nm); (d) as in (c) after photolysis ($\lambda > 420$ nm); (e) as in (d) after photolysis ($240 < \lambda < 380$ nm); (f) as in (e) after annealing to 28 K; (g) Fe + 1.0% C_2D_6 in Ar codeposited for 1 h; (h) as in (g) after photolysis ($\lambda > 420$ nm); (i) as in (h) after photolysis ($240 < \lambda < 380$ nm); (j) as in (i) after annealing to 28 K. **i** denotes the product absorption, and **c** indicates bands common to this precursor with different laser-ablated metals.

singlet electronic states, respectively.) The last is not a methylidyne complex, as the C−Fe bond length is 1.923 Å. Finally, the computed structure for the unobserved higher energy CH_2═FeHF (T) complex shows no evidence of agostic distortion, in contrast to the analogous group 6 methylidenes,[22] but the H atom bonded to Fe is tilted back toward carbon.

Fe + C_2H_6. Figure 2 illustrates the ethane reaction product spectra in the Fe−H stretching and C−Fe stretching regions. The sharp Fe−H stretching **i** absorption at 1662.8 and 1660.5 cm^{-1} has the D counterpart at 1196.8 cm^{-1} (H/D ratio of 1.387). They decrease slightly on visible irradiation but almost triple in the following UV irradiation, and their frequencies are compared with FeH_2 and FeD_2 absorptions of 1660.8 and 1204.2 cm^{-1}.[24] The Fe−H stretching absorption indicates formation of an insertion complex (CH_3CH_2−FeH), parallel to the cases of Fe + CH_4 and Fe + CH_3F. A weak **i** absorption observed at 482.9 cm^{-1} is assigned to the C−Fe stretching mode without observation of the deuterium counterpart. The observed frequencies match well with the DFT frequencies as shown in Table S2 (Supporting Information). The broader 1672 and 1220 cm^{-1} bands increase on annealing and are believed due to ethane precursor perturbations of the insertion complex. The Fe−H stretching frequency for ethyl−FeH is about 10 cm^{-1} higher than for the methyl−FeH counterpart,[8] and the C−Fe stretch is about 38 cm^{-1} lower.

Fe + CH_2X_2 (X = F, Cl). Figure 3 shows the CH_2F_2 and CH_2FCl spectra in the C−F stretching and low-frequency regions, and frequencies are given in Table 2. Unlike the cases of CH_3F and C_2H_6, two sets of product absorptions (**i** and **m** for insertion and methylidene products) are observed in all methylene halide spectra, showing that α-halogen migration is favorable in the reaction with CH_2X_2. In the methylene fluoride spectra, the **i** absorptions increase 30, 20, and another 20% (total 70%) on visible, UV, and full arc irradiations, respectively. The **m** absorptions, on the other hand, slightly decrease on visible and full arc photolysis but increase about 30% on UV photolysis. The **i** absorption at 937.0 cm^{-1} with its deuterium counterpart at 915.5 cm^{-1} (H/D ratio of 1.023) is assigned to the C−F stretching mode of CH_2F−FeF on the basis of its frequency and small D shift. Another **i** absorption observed at 666.0 cm^{-1} is assigned to the Fe−F stretching mode, whereas the CD_2F−FeF counterpart (expected at 4 cm^{-1} lower) is evidently covered by residual CO_2 absorption. Table S3 (Supporting Information) shows good correlation between the matrix infrared and DFT calculated frequencies, especially for the unusually low C−F stretching frequency.

The **m** absorptions are all observed below 700 cm^{-1}, indicating the absence of a C−F bond in the product responsible for the **m** absorptions. The strong **m** absorptions at 695.3 and 689.2 cm^{-1} along with the deuterium counterparts at 691.3 and 688.1 cm^{-1} are assigned to the FeF_2 antisymmetric stretching mode of CH_2═FeF_2 on the basis of the frequencies and small shifts of deuterium substitution. The weaker absorptions at 594.0

(24) (a) Rubinovitz, R. L.; Nixon, E. R. *J. Phys. Chem.* **1986**, *90*, 1940. (b) Chertihin, G. V.; Andrews, L. *J. Phys. Chem.* **1995**, *99*, 12131 (FeH_2).

Table 2. Frequencies of Product Absorptions Observed from Reactions of Fe with Methylene Halide (CH_2X_2, X = F, Cl) Isotopomers in Excess Argon[a]

CH_2F_2	CD_2F_2	CH_2FCl	CD_2FCl	CH_2Cl_2	CD_2Cl_2	$^{13}CH_2Cl_2$	description
				Group **i**			
				1380.1	1023.9	1376.1	CH_2 scis
				552.9		549.6	CH_2 rock
		514.4	477.2	580.0	553.9	567.7	C−Fe str
937.0	915.5	927.1	903.3	543.3	525.3	538.2	C−X str
666.0							Fe−X str
				Group **m**			
			671.9		610.9		CH_2 wag
506.1		532.2		599.0		594.1	CH_2 rock
		615.3					C═Fe str
695.3, 689.2	691.3, 688.1	678.5		480.3, 477.5, 474.5	478.6, 475.7, 472.8	480.3, 477.4, 474.4	FeX_2 asym str
594.0							FeX_2 sym str

[a] All frequencies are in cm^{-1}. The description gives the major coordinate, and **i** and **m** denote insertion and methylidene products, respectively.

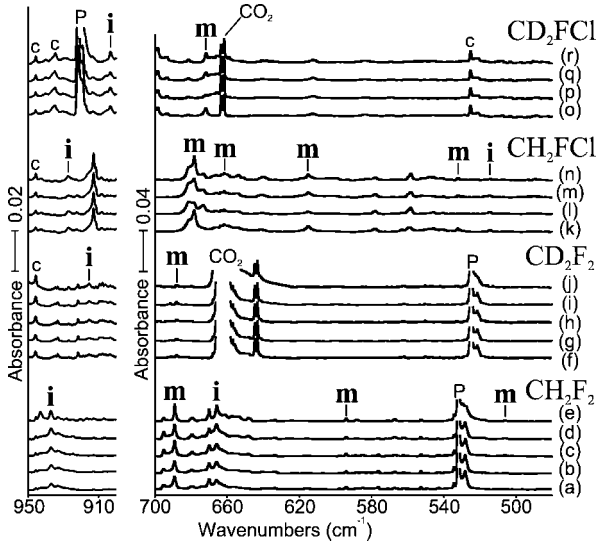

Figure 3. IR spectra in the regions of 950−900 and 700−480 cm^{-1} for laser-ablated Fe atoms codeposited with CH_2F_2 and CH_2FCl isotopomers in excess argon at 10 K and their variation: (a) Fe + 0.5% CH_2F_2 in Ar codeposited for 1 h; (b) as in (a) after photolysis (λ > 420 nm); (c) as in (b) after photolysis (240 < λ < 380 nm); (d) as in (c) after photolysis (λ > 220 nm); (e) as in (d) after annealing to 28 K; (f) Fe + 0.5% CD_2F_2 in Ar codeposited for 1 h; (g) as in (f) after photolysis (λ < 420 nm); (h) as in (g) after photolysis (240 < λ < 380 nm); (i) as in (h) after photolysis (λ > 220 nm); (j) as in (i) after annealing to 28 K; (k) Fe + 0.5% CH_2FCl in Ar codeposited for 1 h; (l) as in (k) after photolysis (λ > 420 nm); (m) as in (l) after photolysis (240 < λ < 380 nm); (n) as in (m) after annealing to 28 K; (o) Fe + 0.5% CD_2FCl in Ar codeposited for 1 h; (p) as in (o) after photolysis (λ > 420 nm); (q) as in (p) after photolysis (240 < λ < 380 nm); (r) as in (q) after annealing to 28 K. **i** and **m** denote the product absorption groups. CO_2, c, and P indicate residual CO_2, bands common to this precursor and different metals, and precursor absorptions, respectively.

and 506.1 cm^{-1} are designated to the symmetric FeF_2 stretching and CH_2 rocking modes without observation of the deuterium counterparts. Table S4 (Supporting Information) shows that all other bands are much weaker and provides good correlation for the observed and DFT values, supporting formation of the higher oxidation state product, $CH_2{=}FeF_2$. Our B3LYP calculations also show that $CH_2F{-}FeF$ (Q) and $CH_2{=}FeF_2$ (T) are 49 and 45 kcal/mol more stable than the reactants, but $CH{\equiv}FeHF_2$ (S) is almost 90 kcal/mol higher energy than $CH_2{=}FeF_2$ (T). Ligand-stabilized iron carbene complexes are rare, and many of their structural properties remain to be explored.[4] The present result shows that the reaction of small haloalkanes with laser-ablated Fe atoms turns out to be an effective way to form very simple iron carbenes via C−X insertion and subsequent α-halogen migration.

The product absorptions in the CH_2FCl spectra in Figure 3 are stronger, which suggests that C−Cl insertion may be faster than C−F insertion, as the chlorine electron cloud cross-section is larger than that for fluorine (the reactions with CH_2FCl are computed to be only 20% more exothermic than the analogous CH_2F_2 reactions). The **i** absorptions remain unchanged on visible photolysis but decrease 70% on the following UV photolysis and later partly recover in the early stage of annealing. The **m** absorptions, on the other hand, decrease 50% on visible photolysis but recover on the following UV photolysis. The **i** absorption at 927.1 cm^{-1} and its deuterium counterpart at 903.3 cm^{-1} are slightly lower than the C−F stretching frequencies of $CH_2F{-}FeF$, and they are assigned to the C−F stretching modes of $CH_2F{-}FeCl$ and $CD_2F{-}FeCl$. Another **i** absorption at 514.4 cm^{-1} is assigned to the C−Fe stretching mode of $CH_2F{-}FeCl$ with the $CD_2F{-}FeCl$ counterpart at 477.2 cm^{-1}.

The relatively strong **m** absorption at 678.5 cm^{-1} is assigned to the Fe−F stretching mode of $CH_2{=}FeFCl$. The strong coupling between the Fe−F stretching and CH_2 wagging modes results in a large variation in intensity of the bands upon deuteration, as shown in Table S6 (Supporting Information). The absorption at 671.9 cm^{-1} in the CD_2FCl spectra is assigned to the CH_2 wagging mode, while the H counterpart expected at about 705 cm^{-1} is believed to be covered by a precursor absorption. The **m** absorptions at 615.3 and 532.2 cm^{-1} in the CH_2FCl spectra are assigned to the C−Fe stretching and CH_2 rocking modes without observation of the D counterparts. The insertion and carbene complexes are 58 and 54 kcal/mol more stable than the reactants.

Figures S1 and 4 show the CH_2Cl_2 spectra in the CH_2 bending and Fe−Cl stretching regions. The **i** and **m** absorptions show reversible intensity changes on irradiation. With visible light, the **i** absorptions double their original intensities, but the **m** absorptions almost disappear. However, on the following UV irradiation the **i** absorptions decrease back to their original intensities, but the **m** absorptions increase to 3 times as strong as their original intensities. They repeat these variations in intensity on the following cycle of visible and UV irradiation. This photoreversibility suggests that the products responsible for the **i** and **m** absorptions are interconvertible during the process of irradiation.

The **i** absorption at 1380.1 cm^{-1} along with its D and ^{13}C counterparts at 1023.9 and 1376.1 cm^{-1} (H/D and $^{12}C/^{13}C$ ratios of 1.348 and 1.003) is assigned to the CH_2 scissoring mode of $CH_2Cl{-}FeCl$ on the basis of the frequency and the large D and small ^{13}C shifts. The CH_2 scissoring band of $CH_2{=}FeCl_2$ would

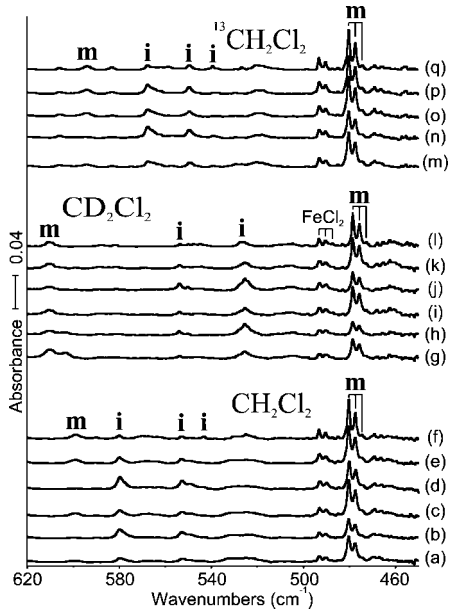

Figure 4. IR spectra in the 620−450 cm^{-1} region for laser-ablated Fe atoms codeposited with methylene chloride isotopomers in excess argon at 10 K and their variations: (a) Fe + 0.5% CH_2Cl_2 in Ar codeposited for 1 h; (b) as in (a) after photolysis ($\lambda > 420$ nm); (c) as in (b) after photolysis ($240 < \lambda < 380$ nm); (d) as in (c) after photolysis ($\lambda > 420$ nm); (e) as in (d) after photolysis ($240 < \lambda < 380$ nm); (f) as in (e) after annealing to 28 K; (g) Fe + 0.5% CD_2Cl_2 in Ar codeposited for 1 h; (h) as in (g) after photolysis ($\lambda > 420$ nm); (i) as in (h) after photolysis ($240 < \lambda < 380$ nm); (j) as in (i) after photolysis ($\lambda > 420$ nm); (k) as in (j) after photolysis ($240 < \lambda < 380$ nm); (l) as in (k) after annealing to 28 K; (m) Fe + 0.5% $^{13}CH_2Cl_2$ in Ar codeposited for 1 h; (n) as in (m) after photolysis ($\lambda > 420$ nm); (o) as in (n) after photolysis ($240 < \lambda < 380$ nm); (p) as in (o) after photolysis ($\lambda > 220$ nm); (q) as in (p) after annealing to 28 K. **i** and **m** denote the product absorption groups.

appear in the region about 130 cm^{-1} lower (see Table S8 in the Supporting Information). Another **i** absorption at 580.0 cm^{-1} with relatively small D and sizable ^{13}C shifts of −26.1 and −12.3 cm^{-1} (H/D and $^{12}C/^{13}C$ ratios of 1.047 and 1.022) are characteristic of the C−Fe stretching mode. Another **i** absorption at 552.9 cm^{-1} along with its ^{13}C counterpart at 549.6 cm^{-1} ($^{12}C/^{13}C$ ratio of 1.006) is assigned to the CH_2 rocking mode, while the deuterium counterpart is apparently beyond our observation range. The **i** absorption at 543.3 cm^{-1} has its D and ^{13}C counterparts at 525.3 and 538.2 cm^{-1}, which are appropriate for the C−Cl stretching mode. The low C−Cl stretching frequency suggests an unusually weak C−Cl bond, which will be discussed in Fe Product Structures. Our reasonable agreement of observed and DFT calculated frequencies is shown in Table S7 (Supporting Information).

The three strong absorptions with intensity ratio of about 9/6/1 at 480.3, 477.5, and 474.5 cm^{-1} have similarly split D and ^{13}C counterparts at 478.6, 475.7, and 472.8 cm^{-1} and at 480.3, 477.4, and 474.4 cm^{-1}. Such a 9/6/1 triplet pattern identifies the motion of two equivalent chlorine atoms. This is an antisymmetric $FeCl_2$ stretching mode on the basis of the frequencies, isotopic shifts, and statistical chlorine isotopic weights, which provides strong evidence for formation of a product with two equivalent Cl atoms in a $FeCl_2$ group. The differences in frequency of 2.8 and 3.0 cm^{-1} between the neighboring absorptions also exactly match with the B3LYP values of 2.8 and 3.0 cm^{-1} and the BPW91 values of 2.9 and 3.0 cm^{-1}. Note below that the isolated $FeCl_2$ molecule absorption is only 13 cm^{-1} higher. Another **m** absorption at 599.0 cm^{-1} with a ^{13}C shift of −4.9 cm^{-1} is appropriate for a CH_2 motion, and the rock is computed at 519 cm^{-1} for the triplet state but higher at 554 cm^{-1} for the quintet state. This agreement is poor owing to mode mixing with the quintet state, as the strongest quintet state modes fall in this region (Table S8 footnote). The deuterium counterpart of another mode observed at 610.9 cm^{-1} in the CD_2Cl_2 spectra is assigned to the CD_2 wagging mode, which is computed in this region (Table S8), while the H and ^{13}C counterparts are covered by the strong precursor C−Cl stretching absorptions.

The correlation of the diagnostic $FeCl_2$ stretching mode with the BPW91 and B3LYP calculated values is good enough to suggest identification of the interesting $CH_2{=}FeCl_2$ iron carbene molecule, but differences between other frequencies computed with these two density functionals and the 2.63 and 2.23 spin expectation values for the triplet state using two functionals all point to the multireference nature of this molecule and the approximation provided by density functional theory. The quintet state $CH_2{-}FeCl_2$ molecule is isoergic at the B3LYP level and 7 kcal/mol higher than the triplet $CH_2{=}FeCl_2$ ground state (BPW91), and the C−Fe bond length is 0.13 Å (B3LYP) or 0.15 (BPW91) longer in the quintet state. The molecule we observe in solid argon is probably a mixed configuration dominated by these two low-energy states. The reversible photochemical equilibrium established with the above insertion product $CH_2Cl{-}FeCl$ also supports formation of the carbene product.

The common set of absorptions at 493.2, 490.3, and 487.3 cm^{-1} with intensity ratio of about 9:6:1 in the methylene chloride spectra remain the same in the process of irradiation and are due to the $FeCl_2$ molecule byproduct, on the basis of agreement within 0.2 cm^{-1} to reported frequencies[25b] for this stable triatomic molecule isolated in solid argon.[25] The $FeCl_2$ absorptions are not observed in the CH_2FCl spectra but appear in the spectra from iron reactions with $CHCl_3$ and CCl_4 to be described below, indicating that $FeCl_2$ is a byproduct of the atomic Fe reaction with the precursor.

Again, the product energies relative to the Fe(^{5}D) and CH_2Cl_2 reagents help to understand the yield of products. Figure 4 shows a comparable yield of the first insertion product $H_2ClC{-}FeCl$ and the methylidene $CH_2{=}FeCl_2$, which are respectively 68 and 60 kcal/mol lower in energy than the reagents. On the other hand, triplet $HC{\equiv}FeHCl_2$ with no symmetry converged to the methylidene, and calculation for the singlet $HC{\equiv}FeHCl_2$ methylidyne in C_s symmetry finds a transition state with 41 kcal/mol higher energy than the reagents. Thus, the methylidyne complex is not a stable species.

An interesting photochemical rearrangement is observed for the two methylene chloride reaction products, which takes advantage of the Cl lone-pair interaction with Fe in the insertion product to assist the Cl transfer to Fe in the methylidene complex. Ultraviolet irradiation initiates rearrangement to the slightly higher energy methylidene, and visible light reverses this process (eq 1). The observation of isolated $FeCl_2$ absorptions here is important as an insightful byproduct of the iron and dichloromethane reaction.

$$Fe + CH_2Cl_2 \rightarrow H_2ClC{-}FeCl \underset{vis}{\overset{UV}{\rightleftharpoons}} CH_2{=}FeCl_2 \qquad (1)$$

Fe + CHX_3. Figure 5 illustrates the CHF_3 spectra, where only one group of absorptions is observed, and values are given in Table 3. The **m** absorptions at 1161.2 and 925.0 cm^{-1} in the CDF_3 spectra are assigned to the coupled C−F stretching and

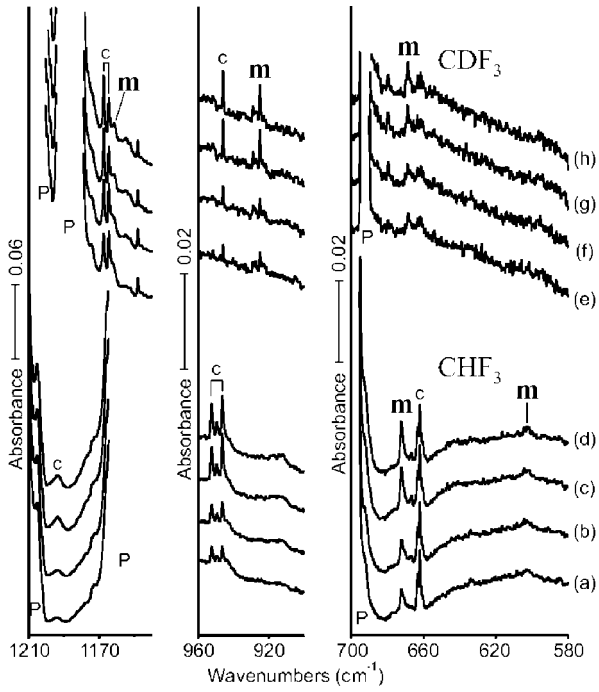

Figure 5. IR spectra in the regions of 1210−1140, 960−900, and 700−580 cm^{-1} for laser-ablated Fe atoms codeposited with fluoroform isotopomers in excess argon at 10 K and their variations. (a) Fe + 0.5% HCF_3 in Ar codeposited for 1 h; (b) as in (a) after photolysis (λ < 290 nm); (c) as in (b) after photolysis (λ < 220 nm); (d) as in (c) after annealing to 30 K; (e) Fe + 0.5% DCF_3 in Ar codeposited for 1 h; (f) as in (e) after photolysis (λ < 290 nm); (g) as in (f) after photolysis (λ < 220 nm); (h) as in (g) after annealing to 30 K. **m** denotes the product absorption. P and c designate the precursor and bands common to this precursor with different laser-ablated metals.

Table 3. Frequencies of Product Absorptions Observed from Reactions of Fe and with Haloform (CHX_3, X = F, Cl) Isotopomers in Excess Argon[a]

CHF_3	CDF_3	$CHCl_3$	$CDCl_3$	$^{13}CHCl_3$	description
			Group **i**		
		1187.9	871.4	1185.9	C−H bend
		510.5, 507.5	498.0	501.9	C−X str
			Group **m**		
	925.0	1083.4		1036.4	HCFe bend
		540		534	C═Fe str
	1161.2	870.3, 865.6	804.7, 798.3	849.6, 845.5	C−X str
672.2	668.8	453.1	452.0	452.9	FeX_2 asym str
602.0					FeX_2 sym str

[a] All frequencies are in cm^{-1}. The description gives the major coordinate, and **i** and **m** stand for insertion and methylidene products, respectively.

DCF bending modes of CDF═FeF_2 on the basis of the frequency positions and DFT calculations, while the H counterparts expected at about 1138 and 1239 cm^{-1} are evidently covered by precursor absorptions (Table S10, Supporting Information). The strong **m** absorption at 672.2 cm^{-1} and its counterpart at 668.8 cm^{-1} in the deuterium-substituted species (H/D ratio of 1.005) are due to the FeF_2 antisymmetric stretching mode on the basis of their frequency and the small deuterium shift. The weak **m** absorption at 602.0 cm^{-1} is tentatively assigned to the symmetric FeF_2 stretching mode. Correlation of the observed frequencies with the DFT values substantiate formation of the simple methylidene complex (CHF═FeF_2), particularly the coupled C−F stretch, DCF bending pair of bands. It should be pointed out here that the above frequencies cannot be assigned to the corresponding **i** species CHF_2−FeF, since the diagnostic 1161.2 and 925.0 cm^{-1} bands in the CDF_3 spectra are not compatible with the frequencies computed for CDF_2−FeF (Table S9, Supporting Information; the calculated value of the strongest band is 88 cm^{-1} lower than our observed value), and accordingly this insertion product is not observed in our experiments.

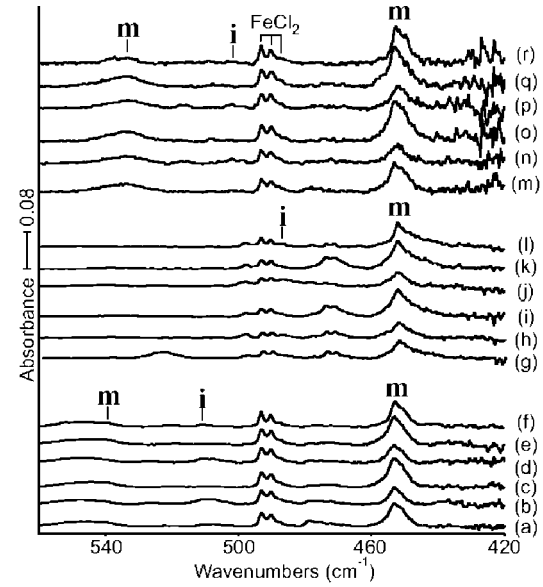

Figure 6. IR spectra in the 560−420 cm^{-1} region for laser-ablated Fe atoms codeposited with chloroform isotopomers in excess argon at 10 K and their variations: (a) Fe + 0.5% $HCCl_3$ in Ar codeposited for 1 h; (b) as in (a) after photolysis (λ > 420 nm); (c) as in (b) after photolysis (240 < λ < 380 nm); (d) as in (c) after photolysis (λ > 420 nm); (e) as in (d) after photolysis (240 < λ < 380 nm); (f) as in (e) after annealing to 28 K; (g) Fe + 0.5% $DCCl_3$ in Ar codeposited for 1 h; (h) as in (g) after photolysis (λ > 420 nm). (i) as in (h) after photolysis (240 < λ < 380 nm); (j) as in (i) after photolysis (λ > 420 nm); (k) as in (j) after photolysis (240 < λ < 380 nm); (l) as in (k) after annealing to 28 K; (m) Fe + 0.5% $H^{13}CCl_3$ in Ar codeposited for 1 h; (n) as in (m) after photolysis (λ > 420 nm); (o) as in (n) after photolysis (240 < λ < 380 nm); (p) as in (o) after photolysis (λ > 420 nm); (q) as in (p) after photolysis (240 < λ < 380 nm); (r) as in (q) after annealing to 28 K. **i** and **m** denote the product absorption groups.

Apparently, we did not trap the CHF_2−FeF intermediate, which is 42 kcal/mol lower than Fe + CHF_3, although the final CHF═FeF_2 product is 37 kcal/mol lower in energy than the reagents at the B3LYP level of theory. However, the chloroform reaction is more exothermic and gives a higher yield, and both products are observed.

Shown in Figures S2 (Supporting Information) and 6 are the $CHCl_3$ spectra, where the **m** absorptions are relatively stronger than **i** absorptions. The **i** absorption intensities almost triple on visible photolysis, while the **m** absorption intensities halve. The **i** absorptions, however, nearly disappear after UV photolysis, whereas the **m** absorptions dramatically increase to become 30% stronger than their original intensity. Similar changes in intensity repeat in the following cycle of visible and UV irradiations. This photoreversibility, parallel to the case of Fe + CH_2Cl_2, suggests interconversion between the insertion and carbene products (eq 2). The **i** absorption at 1187.9 cm^{-1} has a D

(25) (a) Thompson, K. R.; Carlson, K. D. *J. Chem. Phys.* **1968**, *49*, 4379. (b) Jacox, M. E.; Milligan, D. E. *J. Chem. Phys.* **1969**, *51*, 4143. (c) Hastie, J. W.; Hauge, R. H.; Margrave, J. L. *High Temp. Sci.* **1971**, *3*, 257. (d) Green, D. W.; McDermott, D. P.; Bergman, A *J. Mol. Spectrosc.* **1983**, *98*, 111 ($FeCl_2$).

counterpart at 871.4 cm^{-1} (needs amplification of the compressed spectrum in Figure S2) and a ^{13}C component at 1185.9 cm^{-1}, and these bands are assigned to the C−H bending mode of $CHCl_2$−FeCl, which is 64 kcal/mol lower energy than Fe + $CHCl_3$, on the basis of the large D and small ^{13}C shifts (Table S11, Supporting Information). Another **i** absorption at 510.5 cm^{-1} with its D and ^{13}C counterparts at 498.0 and 501.9 cm^{-1} (H/D and $^{12}C/^{13}C$ ratios of 1.025 and 1.017) is assigned to the C−Fe stretching mode of the insertion complex ($CHCl_2$−FeCl) due to the frequency and sizable ^{13}C shift. Unfortunately, other **i** absorptions are covered, are too weak, or are beyond our observation range on the basis of the prediction of calculations (Table S11).

$$Fe + CHCl_3 \rightarrow HCl_2C{-}FeCl \underset{vis}{\overset{UV}{\rightleftharpoons}} CHCl{=}FeCl_2 \qquad (2)$$

On the other hand, with higher product yield more and stronger **m** absorptions are observed, and triplet CHCl=$FeCl_2$ is 72 kcal/mol lower in energy than the combined reagents. The **m** absorption at 1083.4 cm^{-1} with its ^{13}C counterpart at 1036.4 cm^{-1} is assigned to the HCFe bending mode of CHCl=$FeCl_2$ without observation of the D counterpart (Tables 3 and S12 (Supporting Information)). The strong **m** absorptions at 870.3 and 865.6 cm^{-1} with their D and ^{13}C counterparts at 804.7 and 798.3 cm^{-1} and at 849.6 and 845.5 cm^{-1} (H/D and $^{12}C/^{13}C$ ratios of 1.083 and 1.024) are assigned to the C−Cl stretching mode on the basis of the frequencies and the sizable ^{13}C shifts. A broad **m** absorption and its ^{13}C counterpart at 540 and 534 cm^{-1} ($^{12}C/^{13}C$ ratio of 1.011) are tentatively assigned to the C−Fe stretching modes. The strong **m** absorption at 453.1 cm^{-1} has D and ^{13}C counterparts peaking at 452.0 and 452.9 cm^{-1}, and they are assigned to the $FeCl_2$ antisymmetric stretching mode of CHCl=$FeCl_2$. These **m** isotopic absorptions, unlike the CH_2=$FeCl_2$ bands split into 9/6/1 triplets, are not resolved in this larger molecule. Finally, the very good correlation between observed and calculated frequencies includes four intense IR bands that are within 4.4, 0.5, 3.7, and 2.4% of the B3LYP calculated values and the correct isotopic shifts for the C−Cl stretching mode in the CHCl functional group, including interaction with the C−H(D) bending mode, supports this assignment.

Fe + CX_4. Figure 7 illustrates the CF_3Cl, $^{13}CF_3Cl$, and CF_2Cl_2 spectra in the C−F stretching and low-frequency regions, where the product absorptions marked **i** and **m** are much stronger than the cases described above; values are given in Table 4. The intensities of both **i** absorptions in the CF_3Cl spectra increase about 20% on visible irradiation, while the **m** absorptions remain unchanged. The former, however, decrease to 30% of the original intensity and almost disappear on UV and full arc irradiations, and the latter increase about 40% on UV irradiation and slightly more on full arc irradiation. The **i** absorptions are believed to arise from CF_3−FeCl. The broad **i** absorption at 1014 cm^{-1} with its ^{13}C counterpart at 992 cm^{-1} ($^{12}C/^{13}C$ ratio of 1.022) is assigned to the nearly degenerate A′ and A″ CF_3 stretching modes. The C_s structure of CF_3−FeCl is close to a C_{3v} structure, as shown in Figure 9. Another **i** absorption at 450 cm^{-1} shows a negligible ^{13}C shift and is assigned to the Fe−Cl stretching mode.

The strong **m** absorptions at 1249.9 and 1249.2 cm^{-1} with the ^{13}C counterparts at 1218.0 and 1215.3 cm^{-1} ($^{12}C/^{13}C$ ratios of 1.025 and 1.028) are designated to the symmetric CF_2 stretching mode of CF_2=FeFCl on the basis of the frequencies, substantial ^{13}C shift, and agreement with DFT values. Another **m** absorption pair at 1230.4 and 1227.7 cm^{-1} has their ^{13}C counterparts at 1198.9 and 1196.2 cm^{-1} ($^{12}C/^{13}C$ ratios of 1.026 for both) and are assigned to the antisymmetric CF_2 stretching mode. Another **m** absorption at 658.4 cm^{-1} with its ^{13}C counterpart at 658.1 cm^{-1} is assigned to the CF_2 scissoring mode on the basis of the frequencies, small ^{13}C shift, and relatively low intensity. The strong **m** absorption at 649.1 cm^{-1} shows a negligible ^{13}C shift and is assigned to the Fe−F stretching mode, due to the high intensity and negligible isotopic shift. Again the correlation with DFT values as shown in Table S14 (Supporting Information) substantiate formation of the higher oxidation state complex (CF_2=FeFCl).

Only **m** absorptions are observed in the CF_2Cl_2 spectra. The strong **m** absorption pair split by the matrix at 1246.4 and 1244.3 cm^{-1}, whose frequencies are slightly lower than the corresponding bands in the CF_3Cl spectra, is assigned to the CF_2 symmetric stretching mode of CF_2FeCl_2. Another **m** absorption on the red side at 1220.7 cm^{-1} is assigned to the antisymmetric stretching mode. The group of strong **m** absorptions partially resolved at 463.3, 460.3, and 457.3 cm^{-1} with the intensity ratio

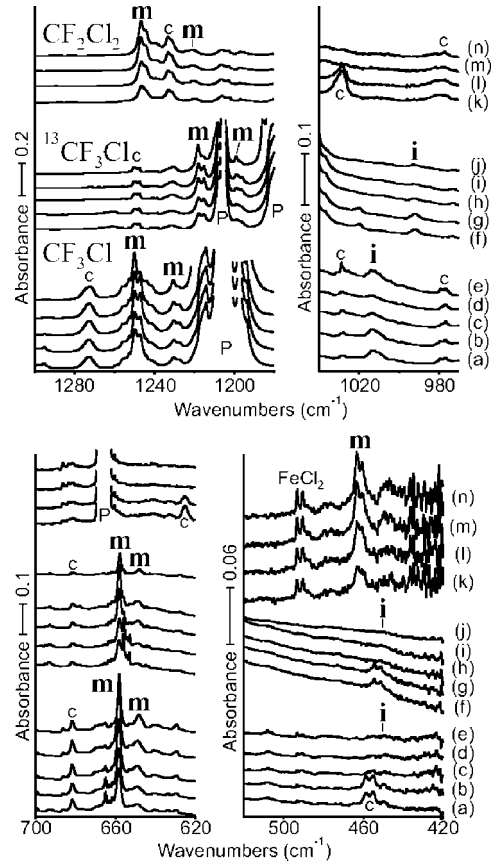

Figure 7. IR spectra in the regions of 1300−1180, 1040−970, 700−620, and 520−420 cm^{-1} for laser-ablated Fe atoms codeposited with CF_3Cl isotopomers and CF_2Cl_2 in excess argon at 10 K and their variations: (a) Fe + 0.5% CF_2Cl_2 in Ar codeposited for 1 h; (b) as in (a) after photolysis (λ < 290 nm); (c) as in (b) after photolysis (λ < 220 nm); (d) as in (c) after annealing to 30 K; (e) Fe + 0.5% CF_3Cl in Ar codeposited for 1 h; (f) as in (e) after photolysis (λ > 420 nm); (g) as in (f) after photolysis (240 < λ < 380 nm); (h) as in (g) after photolysis (λ > 220 nm); (i) as in (h) after annealing to 28 K; (j) Fe + 0.5% $^{13}CF_3Cl$ in Ar codeposited for 1 h; (k) as in (j) after photolysis (λ > 420 nm); (l) as in (k) after photolysis (240 < λ < 380 nm); (m) as in (l) after photolysis (λ > 220 nm); (n) as in (m) after annealing to 28 K. **i** and **m** denote the product absorption groups, and P and c designate the precursor and bands common to this precursor with different laser-ablated metals, respectively.

Table 4. Frequencies of Product Absorptions Observed from Reactions of Fe with Carbon Tetrahalide (CX_4, X = F, Cl) Isotopomers in Excess Argon[a]

CF_3Cl	$^{13}CF_3Cl$	CF_2Cl_2	CCl_4	$^{13}CCl_4$	description
		Group **i**			
1013.5	992.0		637	618	A″ CX_3 str
1010.2					A′ CX_3 str
449.7	449.7				A′ Fe−X str
		Group **m**			
1249.9, 1249.2	1218.0, 1215.3	1246.4, 1244.3	860.4	832.6	CX_2 sym str
1230.4, 1227.7	1198.9, 1196.2	1220.7	838.7	812.5	CX_2 asym str
658.4	658.1				CX_2 bend
649.1	649.0	463.3, 460.3, 457.3	456.5	456.5	FeX_2 asym str
			473.0, 470.1	473.0, 470.1	(pert.) $FeCl_2$

[a] All frequencies are in cm^{-1}. The description gives the major coordinate, and **i** and **m** stand for insertion and methylidene products, respectively.

of 9/6/1 in agreement with the statistical isotopic ratio for two equivalent chlorine atoms is assigned to the antisymmetric $FeCl_2$ stretching mode. It is notable that geometry optimization for the insertion product ends up with carbene complexes in both the quintet and triplet states (Figure 10). CF_2-FeCl_2 (Q) is 6 kcal/mol (B3LYP) lower in energy than $CF_2{=}FeCl_2$ (T), the C−Fe bond length is 0.424 Å longer in the quintet (Figure 10), and their vibrational characteristics are very similar and correlate equally well with the observed spectrum (Tables S13 and S14, Supporting Information). Further multiconfiguration investigation is needed to determine the ground electronic state of CF_2FeCl_2. It is significant, though, that the above spectroscopic evidence indicates transfer of Cl and not F to the iron center. This is expected, as the $CCl_2{=}FeF_2$ isomer is 16 kcal/mol higher in energy (B3LYP), and the computed frequencies for C−Cl modes (876, 845 cm^{-1}) and Fe−F modes (738, 607 cm^{-1}) are quite different from the observed spectrum.

Figure 8 illustrates the CCl_4 and $^{13}CCl_4$ reaction product spectra in the C−Cl and Fe−Cl stretching regions. The 637 cm^{-1} **i** absorption intensity increases about 400% and an additional 100% on visible and UV photolysis, whereas the **m** absorptions halve on visible irradiation and recover some on UV irradiation and at the early stage of annealing. The broad **i** absorption at 637 cm^{-1} with its ^{13}C counterpart at 618 cm^{-1} ($^{12}C/^{13}C$ ratio of 1.031 compared with predicted ratio of 1.034) is assigned to the antisymmetric CCl_3 stretching modes of CCl_3-FeCl, which are predicted within 2 cm^{-1} (B3LYP; Table S15, Supporting Information). The weaker Fe−Cl mode cannot be observed in the low signal 440−420 cm^{-1} region. However, Table S15 shows a considerable difference between the B3LYP and BPW91 frequencies originating from the difference in the predicted structures. This will be discussed more in the Fe Product Structures. The absorption pair at 473.0 and 470.1 cm^{-1} with no measurable ^{13}C shift has the $FeCl_2$ chlorine isotopic profile and is just 20 cm^{-1} lower than isolated $FeCl_2$: this band increases on irradiation and is probably due to $FeCl_2$ perturbed by some other species. Very weak absorption at 442 cm^{-1} has the chlorine isotopic profile and does not change on irradiation, which could be due to $FeCl_3$, but this is just a possibility for consideration.

The strong **m** absorption at 860.4 cm^{-1} shows a ^{13}C shift of −27.8 cm^{-1} ($^{12}C/^{13}C$ ratio of 1.0334) for a C−Cl stretching mode and an unresolved chlorine isotopic contour for two equivalent chlorine atoms, and the related satellite band at 838.7 cm^{-1} exhibits a −26.2 cm^{-1} ^{13}C shift ($^{12}C/^{13}C$ ratio of 1.0322). Another **m** absorption at 456.5 cm^{-1} with no measurable ^{13}C shift is assigned to the antisymmetric $FeCl_2$ stretching mode. Chlorine isotopic splittings are not resolved on the $FeCl_2$ stretching absorption, although the band profile is appropriate, probably because this CCl_2FeCl_2 molecule interacts more strongly with the matrix cage, than for example CH_2FeCl_2, where the isotopic splittings are resolved (Figure 4).

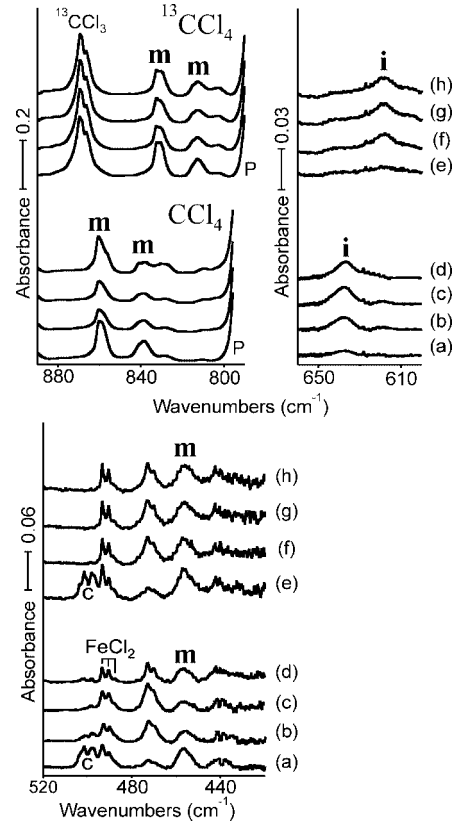

Figure 8. IR spectra in the regions of 790−890, 670−600, and 520−420 cm^{-1} for laser-ablated Fe atoms codeposited with carbon tetrachloride isotopomers in excess argon at 10 K and their variations: (a) Fe + 0.5% CCl_4 in Ar codeposited for 1 h; (b) as in (a) after photolysis ($\lambda > 420$ nm); (c) as in (b) after photolysis ($240 < \lambda < 380$ nm); (d) as in (c) after annealing to 28 K; (e) Fe + 0.5% $^{13}CCl_4$ in Ar codeposited for 1 h; (f) as in (e) after photolysis ($\lambda > 420$ nm); (g) as in (f) after photolysis ($240 < \lambda < 380$ nm); (h) as in (g) after annealing to 28 K. **i** and **m** denote the product absorption groups. P and c designate the precursor and bands common to this precursor with different laser-ablated metals, respectively.

In addition, one Fe experiment with 0.05% CCl_4 in excess hydrogen as the matrix codeposited at 4 K gave a simpler spectrum with better isotopic resolution in the upper region. A 9/6/1 triplet was observed at 858.7, 857.5, and 856.2 cm^{-1} and the first two 9/6 components of the lower band at 840.2, 837.9 cm^{-1}, which are diagnostic for two equivalent chlorine atoms in the CCl_2FeCl_2 product. These absorptions and an associated 452 cm^{-1} band decreased on UV irradiation. Another broad

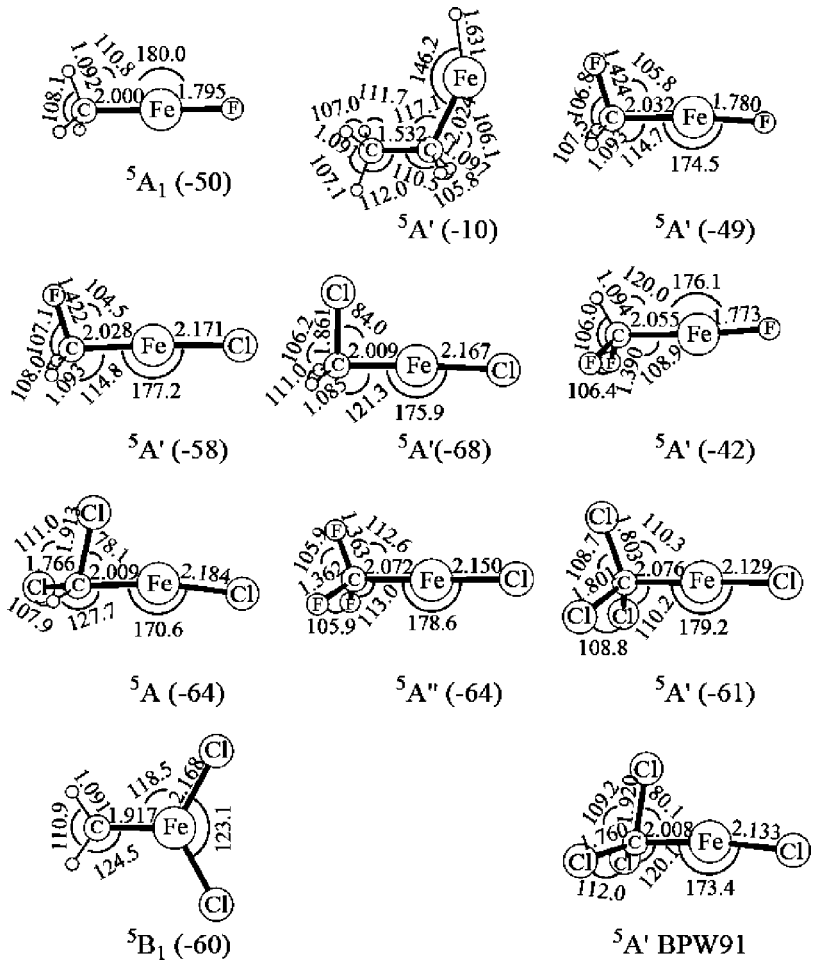

Figure 9. Optimized molecular structures of Fe insertion complexes in the ground quintet states. The structures were calculated with B3LYP/6-311++G(3df,3pd), except for the CCl_3-FeCl structure, which was calculated with BPW91/6-311++G(3df,3pd). CH_3-FeF has a C_{3v} structure, whereas $CHCl_2-FeCl$ has a C_1 structure. Others have C_s structures. The bond lengths and angles are in Å and deg, respectively. The product energy relative to Fe and the parent molecule is given in kcal/mol.

634 cm^{-1} band increased on UV irradiation, which is the insertion product. Interestingly, no band for $FeCl_2$ or a perturbed $FeCl_2$ species was observed in the 470−500 cm^{-1} region, but UV irradiation of the CCl_2FeCl_2 product in solid hydrogen also gave an increased 1755 cm^{-1} absorption for HFeCl.[26]

Tables S16 and S17 (Supporting Information) compare the three observed frequencies with those calculated for the lowest triplet state of $CCl_2{=}FeCl_2$ with a 1.777 Å C−Fe bond length and a 7 kcal/mol lower energy quintet state for CCl_2-FeCl_2 with a longer 1.990 Å C−Fe bond length. The B3LYP frequencies bracket the observed values with the quintet frequencies lower and the triplet results higher. Both calculations reveal slightly larger ^{13}C shifts and smaller ^{37}Cl shifts for the higher frequency mode, which is symmetric CCl_2 stretching, than the lower frequency mode, which is antisymmetric CCl_2 stretching. In fact, the calculated ^{37}Cl shifts for the two triplet state modes are exactly twice that observed for the first band separation, which is expected for the $^{35}Cl,^{35}Cl$ to $^{35}Cl,^{37}Cl$ splitting. The calculated frequencies in Tables S16 and S17 show convincingly that our three observed bands can be assigned to the CCl_2FeCl_2 methylidene molecule and suggest that the ground-state configuration is dominated by mixed triplet and quintet spin states.

The Fe reaction with CCl_4 proceeds through the insertion complex CCl_3-FeCl, which is 61 kcal/mol lower in energy than the reactants, to the 24 kcal/mol lower energy methylidene complex (B3LYP, quintet insertion to triplet methylidene), which is 85 kcal/mol lower than the reagents (eq 3). However, visible irradiation converts some methylidene back to the higher energy insertion complex. Another α-Cl transfer to Fe to form $ClC{\equiv}FeCl_3$ (T) is unfavorable in terms of energy, as this species with real frequencies and a 1.627 Å C−Fe bond length is 21 kcal/mol higher than $CCl_2{=}FeCl_2$ (T) and the S counterpart with a 1.590 Å C−Fe bond length is 40 kcal/mol higher in energy than $CCl_2{=}FeCl_2$ (T). Finally, our search for this iron methylidyne complex was not successful (the strong diagnostic C−Cl stretching mode in the 1200 cm^{-1} region[11] was not observed).

$$Fe + CCl_4 \rightarrow Cl_3C-FeCl \underset{vis}{\rightleftharpoons} CCl_2{=}FeCl_2 \qquad (3)$$

The present results demonstrate that, unlike CH_3F and C_2H_6, the di-, tri-, and tetrahalomethanes form both insertion and carbene complexes in reactions with Fe. Furthermore, the relative yield of **m** to **i** increases with the number of halogens in the precursor. Substitution of hydrogen with halogen efficiently stabilizes the higher oxidation state complex with carbon−metal double bonds, due to the strong metal−halogen bond, particularly for heavier members of the family group.[11,12]

(26) Parker, S. F.; Peden, C. H. F.; Barrett, P. H.; Pearson, R. G. *J. Am. Chem. Soc.* **1984**, *106*, 1304 (HFeCl).

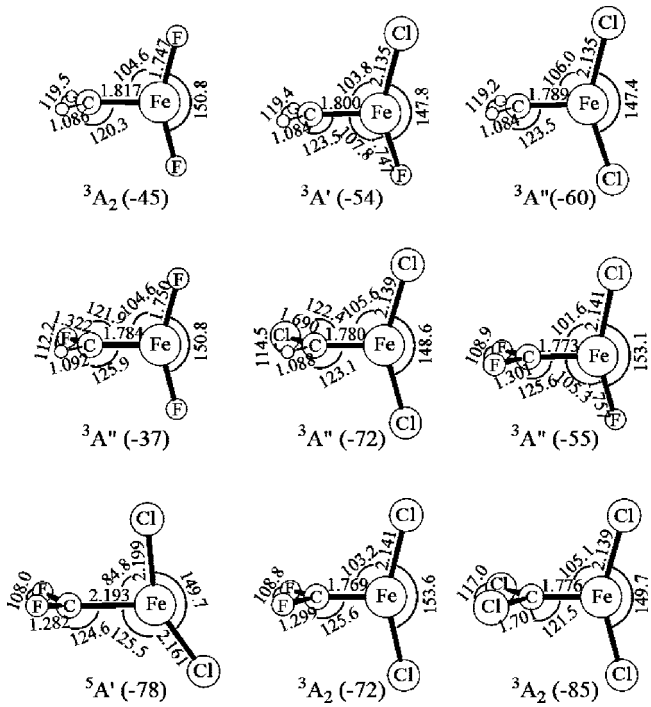

Figure 10. Optimized molecular structures of Fe carbene complexes in the ground triplet states. The structures were calculated with B3LYP/6-311++G(3df,3pd), and they have mutually perpendicular CX_2 and FeX_2 subunits (slight deviations in dihedral angles for CH_2=FeFCl (92.6°), CH_2=$FeCl_2$ (86.6°), CHCl=$FeCl_2$ (91.1°), and CF_2=FeFCl (89.4°)). The C−Fe bond lengths are considerably shorter than those of the insertion complexes. However, the C−Fe bond of CF_2=$FeCl_2$ in the quintet ground state is even longer than those of the insertion complexes, indicating that the single carbon−metal bond is further weakened by the chlorine atom tilted toward the C−Fe bond. The bond lengths and angles are in Å and deg, respectively. The product energy relative to Fe and the parent molecule is given in kcal/mol.

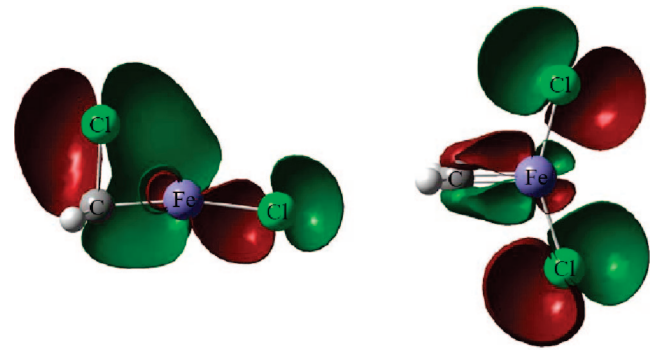

Figure 11. Molecular orbital for the CH_2Cl−FeCl insertion complex showing the chlorine lone pair−iron interaction, which leads to α-Cl transfer and the CH_2=$FeCl_2$ methylidene complex, also illustrated.

However, no iron carbyne product is identified from the matrix infrared spectra. B3LYP calculations also show that, while the energies of the insertion and carbene products are comparable, the carbyne products are significantly higher in energy: the carbyne complexes are 20 kcal/mol or more higher in energy than the carbene products.

Fe Product Structures. Figures 9 and 10 illustrate the structures of Fe insertion, and carbene products examined in this study were calculated at the B3LYP level of theory (except where otherwise noted). While the insertion complexes mostly have a C_s structure in the quintet ground state, it is notable that in CH_2Cl−FeCl and $CHCl_2$−FeCl one of the chlorine atoms is inclined to the Fe atom, showing considerable C−Cl bond distortion, resulting in an unusual C_1 structure in the case of $CHCl_2$−FeCl. Similar structures were also observed in the BPW91 calculations (∠ClCFe = 82.7 and 87.9° for CH_2Cl−FeCl and $CHCl_2$−FeCl). As a result, the C−Cl bonds of CH_2Cl−FeCl and $CHCl_2$−FeCl (1.861 and 1.913 Å) are relatively very long (cf. 1.803 Å for CCl_3−FeCl in Figure 9), which result in the relatively low C−Cl stretching frequency of 543.3 cm^{-1} for CH_2Cl−FeCl (that for $CHCl_2$−FeCl is too low to observe). The B3LYP structure of CCl_3−FeCl is close to C_{3v} symmetry; however, the BPW91 structure clearly shows a C−Cl inclination toward the Fe atom (∠ClCFe = 80.1°), similar to those of CH_2Cl−FeCl and $CHCl_2$−FeCl. It is also described above that the observed frequencies, particularly the A′ CX_3 symmetric stretching frequencies, fit better with the BPW91 frequencies. Therefore, the insertion complexes containing a C−Cl bond in Figure 9 all show the chlorine distortion toward the Fe atom.

An agostic structure is normally observed for a complex containing a C−H bond in the proximity of a metal center: coordination of the σ C−H bonding electrons to the electron-deficient transition-metal atom causes inclination of the C−H bond.[15,27] It is interesting that similar distortion occurs in complexes possessing a C−Cl bond next to a metal center, while no such C−H or C−F distortion is observed from the Fe insertion complexes. Moreover, no such distortion of the C−H(X) bond has been observed from the insertion complexes produced from reactions of transition metals with methane, ethane, and halomethanes, whereas inclination of a C−H bond to the metal center is commonly observed from the carbene products of early transition metals.[15] Clearly, coordination of the electron-rich Cl atom to Fe is highly favored in the insertion complexes, and this is probably due to coordination of chlorine lone pair electrons to the Fe center. The chlorine lone pair molecular orbital for H_2ClC−FeCl illustrated in Figure 11 demonstrates this interaction with the 3d orbitals of the iron center. A continuation of this interaction leads directly to the methylidene complex. Lone-pair bonding effects have been discussed by Clot and Eisenstein, who consider this as different from the agostic interaction.[27d]

The Fe carbenes investigated here, on the other hand, all have allene-type structures with mutually perpendicular CX_2 and FeX_2 subgroups, as shown in Figure 10, in line with those of the previously studied small Ru carbenes, which may be compared with the planar or near-planar structures of the early-transition-metal carbenes.[10,15] The CF_2FeCl_2 structures in the quintet and triplet states are also shown. The carbene in the $^5A'$ state is 6 kcal/mol more stable than in the triplet state, and the observed vibrational characteristics are consistent with the calculated frequencies for both states, which points to a multiconfiguration description. The C−Fe bond in the quintet structure (2.193 Å) is much longer than that in the triplet structure (1.769 Å) and is considered a single bond. It is notable that the relatively long Fe−Cl bond (2.199 Å) is inclined to the CF_2 group. The Fe

(27) (a) Crabtree, R. H. *Chem. Rev.* **1995**, *95*, 987, and references therein. (b) Wada, K.; Craig, B.; Pamplin, C. B.; Legzdins, P.; Patrick, B. O.; Tsyba, I.; Bau, R. *J. Am. Chem. Soc.* **2003**, *125*, 7035. (c) Ujaque, G.; Cooper, A. C.; Maseras, F.; Eisenstein, O.; Caulton, K. G. *J. Am. Chem. Soc.* **1998**, *120*, 361. (d) Clot, E.; Eisenstein, O. In *Computational Inorganic Chemistry*; (Eds.: Kaltzoyannis, N, McGrady, J. E., Eds.; Springer: Heidelberg, Germany, 2004; Structure and Bonding, pp 1−36. (e) Roos, B. O.; Lindh, R.; Cho, H.-G.; Andrews, L. *J. Phys. Chem. A* **2007**, *111*, 6420. (f) Scherer, W.; McGrady, G. S. *Angew. Chem., Int. Ed.* **2004**, *43*, 1782.

carbene complex in the quintet state can be considered as an extreme case of C−Cl lone pair distortion to the Fe center, in line with the Fe insertion complexes containing a C−Cl group, shown in Figure 9 (e.g., CH_2Cl−FeCl and $CHCl_2$−FeCl). The present results illustrate a strong interaction between the C−Cl group and the adjacent Fe atom.

In addition, the analogous CCl_2FeCl_2 molecule also has triplet−quintet multiconfigurational character.

Conclusions

Laser-ablated iron atoms were reacted with halomethanes and ethane, and the products were identified in the matrix infrared spectra on the basis of comparisons with product energies and frequencies calculated with density functional theory. Iron forms insertion complexes in reactions with methyl fluoride and ethane, in line with the previously studied Fe + CH_4 reactions.[8] However, for di-, tri-, and tetrachloromethanes, the matrix spectra contain distinct $FeCl_2$ group absorptions with statistical chlorine isotopic splittings for two equivalent chlorine atom populations and demonstrate the formation of methylidene as well as insertion complexes. Several of these product pairs show interesting photochemical properties, including photoreversibility. The large yield of CH_2═$FeCl_2$ in methylene chloride experiments underscores the favorable C−Cl insertion reaction and α-Cl transfer in these systems. This methylidene species and the CF_2FeCl_2 and CCl_2FeCl_2 analogues appear to contain significant triplet−quintet multiconfigurational character.

Interestingly enough, C−Cl lone pair distortions are observed in the DFT structures of CH_2Cl−-FeCl ($^5A'$), $CHCl_2$−FeCl (^5A), and CCl_3−FeCl ($^5A'$), and the CF_2−$FeCl_2$ ($^5A'$) state shows an extreme case of this distortion, resulting in a carbene structure. This unusual C−Cl distortion and bond elongation evidently results from coordination of the electron-rich Cl atom to the Fe center, as no such distortion was observed for C−H or C−F bonds. While most insertion complexes have a C_s structure, the carbene products all have allene-type structures with no evidence of agostic distortion. Substitution of Cl for F generally increases the reaction yield, suggesting that C−Cl insertion and the following Cl migration are more favorable reactions. In contrast to the group 6 analogues,[22] computed structures for the unobserved higher energy CH_2═FeHF carbene shows no agostic distortion, and the transferred H on Fe is tilted back toward carbon. We hope these density functional investigations of iron methylidene complexes will foster higher level theoretical calculations, in order to understand these interesting interactions and reactive species in more detail.

Acknowledgment. We gratefully acknowledge financial support from the National Science Foundation (U.S.) by Grant No. CHE 03-52487 to L.A. and support from the Korea Institute of Science and Technology Information (KISTI) by Grant No. KSC-2006-S00-2014.

Supporting Information Available: Tables S1−S17, giving calculated product frequencies, and Figures S1 and S2, giving product IR spectra. This material is available free of charge via the Internet at http://pubs.acs.org.

OM8005189